Pion production by protons and ^{3}He on a ^{197}Au target at beam energies of 2.8, 5, 10, and 16.587 GeV/nucleon

Gao-Chan Yong, Xurong Chen, Hu-Shan Xu, and Wei Zuo
Institute of Modern Physics, Chinese Academy of Sciences, Lanzhou 730000, China
(Received 29 June 2011; revised manuscript received 13 December 2011; published 29 February 2012)

Based on a relativistic Boltzmann-Uehling-Uhlenbeck transport model, proton- and ^{3}He-induced reactions on a ^{197}Au target at beam energies of 2.8, 5, 10, and 16.587 GeV/nucleon are studied. It is found that compared with proton-induced reactions, ^{3}He-induced reactions give larger cross sections of pion production, about 5 times those of the proton-induced reactions. And more importantly, pion production from ^{3}He-induced reaction is more inclined to low-angle emission. Neutrino production via positively charged pion is also discussed accordingly.

DOI: 10.1103/PhysRevC.85.024911 PACS number(s): 24.10.Jv, 24.10.Lx, 25.40.Ve, 25.55.−e

I. MOTIVATION

There exists considerable interest in the possibility that one type of neutrino may transform into another type during propagation [1]. It has also been argued that neutrino oscillations are related to stellar collapse [2] and spontaneous parity nonconservation [3]. Nowadays atmospheric [4–6], reactor [7], solar neutrino [8,9], and accelerator neutrinos [10] provide compelling evidence for neutrino mass and oscillation. It is interesting to note that the precise neutrino oscillation parameters have been determined by the KamLAND Collaboration [11] recently. For more about neutrino physics, please see Ref. [12]. In the accelerator-based neutrino experiments, a key issue toward the development of a muon collider or a neutrino beam based on a muon storage ring is the design of a target/capture system capable of capturing a large number of pions. These pions then proceed into a decay channel where the resultant muon decay products are harvested before being conducted into a cooling channel and then subsequently accelerated to the final energy of the facility [13]. Understanding of the production of pions in proton interactions with nuclear targets is thus essential for determining the flux of neutrinos in accelerator-based neutrino experiments [14,15]. A large amount of data was collected by the HARP Collaboration for the above physical subjects recently [16]. In fact, in accelerator-based neutrino experiments, sometimes one needs a ^{3}He-induced reaction. There are many simulation methods focused on such studies, such as the phenomenological Monte Carlo generators GEANT4 [17] and MARS [18] and other theoretical works that have considered more physical processes [19–25]. In this article, after checking the reliability of a relativistic transport model (ART) we made comparative studies of pion production in proton- and ^{3}He-induced reactions on an ^{197}Au target at incident beam energies of 2.8, 5, 10, and 16.587 GeV/nucleon. And finally, we simply discussed neutrino production via positively charged pions.

II. THEORETICAL METHODS

The well-known Boltzmann-Uehling-Uhlenbeck (BUU) model [26] has been used very successful in studying heavy-ion collisions at intermediate energies. The ART model [27] is the relativistic form of the BUU model; in order to simulate heavy-ion collisions at higher energies, some new physics was added. It includes baryon-baryon, baryon-meson, and meson-meson elastic and inelastic scatterings. The ART model includes the following baryons, N, $\Delta(1232)$, $N^*(1440)$, $N^*(1535)$, Λ, and Σ, and mesons, π, ρ, ω, η, and K, as well as their explicit isospin degrees of freedom. Both elastic and inelastic collisions among most of these particles are included. For baryon-baryon scatterings, the ART model includes the following inelastic channels: $NN \leftrightarrow N(\Delta N^*)$, $NN \leftrightarrow \Delta[\Delta N^*(1440)]$, $NN \leftrightarrow NN(\pi\rho\omega)$, $(N\Delta)\Delta \leftrightarrow NN^*$, and $\Delta N^*(1440) \leftrightarrow NN^*(1535)$. In the above, N^* denotes either $N^*(1440)$ or $N^*(1535)$, and the symbol (ΔN^*) denotes a Δ or a N^*. For meson-baryon scatterings, the ART model includes the following reaction channels for the formation and decay of resonances: $\pi N \leftrightarrow [\Delta N^*(1440)N^*(1535)]$ and $\eta N \leftrightarrow N^*(1535)$. There are also elastic scatterings such as $(\pi\rho)(N\Delta N^*) \rightarrow (\pi\rho)(N\Delta N^*)$. For meson-meson interactions, the ART model includes both elastic and inelastic $\pi\pi$ interactions, with the elastic cross section consisting of ρ-meson formation and the remaining part treated as elastic scattering. Also included are reaction channels relevant to kaon production. The extended ART model is one part of a multiphase transport (AMPT) model [28]. We use the Skyrme-type parametrization for the mean field, which reads [27]

$$U(\rho) = A(\rho/\rho_0) + B(\rho/\rho_0)^\sigma, \tag{1}$$

where $\sigma = 7/6$, $A = -0.356$ MeV is attractive, and $B = 0.303$ MeV is repulsive. With these choices, the ground-state compressibility coefficient of nuclear matter $K = 201$ MeV. More details of the model can be found in Ref. [27].

III. RESULTS AND DISCUSSIONS

To check the reliability of using the ART model to study the cross sections of pion production in proton- or ^{3}He-induced reactions, we first made a comparison of pion production in p + Au reaction at an incident beam momentum of 17.5 GeV/c between the theoretical simulations and the E910 data [14] as shown in Fig. 1. The top panel of Fig. 1 shows the inclusive differential cross sections of pion production from p + Au at an incident beam momentum of 17.5 GeV/c. We

 ©2012 American Physical Society

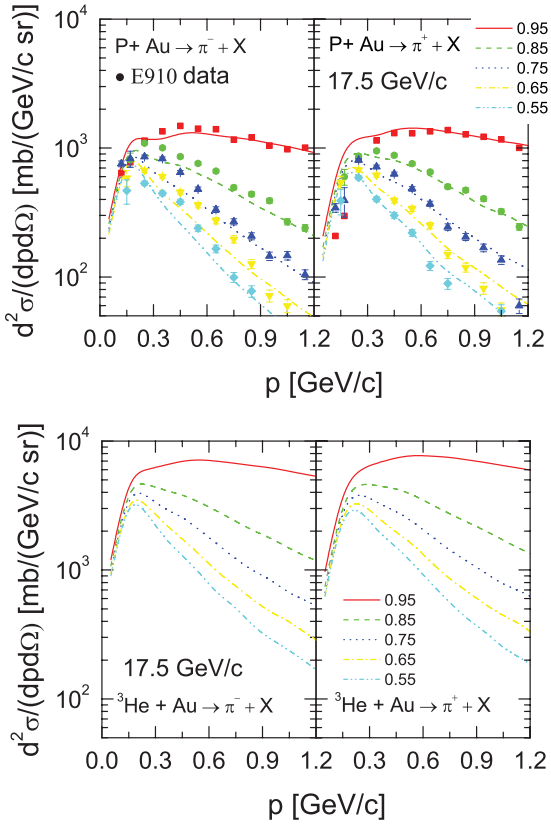

FIG. 1. (Color online) Top: Production cross sections of π^- (left panel) and π^+ (right panel) from $p + \mathrm{Au}$ at the incident beam momentum of 17.5 GeV/c ($E_{\mathrm{beam}} \sim 16.587$ GeV/nucleon) shown in bins of $\cos\theta$ (relative to beam direction). Numbers in the legend refer to the center of each bin. Data are taken from Ref. [14]. Bottom: Same as $p + \mathrm{Au}$ case, but for $^3\mathrm{He} + \mathrm{Au}$.

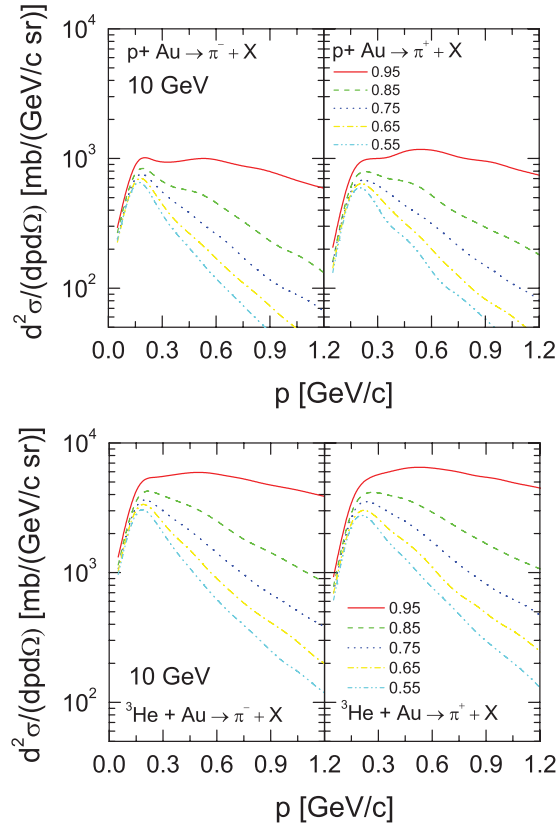

FIG. 2. (Color online) Top: Production cross sections of π^- (left panel) and π^+ (right panel) from $p + \mathrm{Au}$ at an incident beam energy of 10 GeV/nucleon shown in bins of $\cos\theta$. Numbers in the legend refer to the center of each bin. Bottom: Same as the $p + \mathrm{Au}$ case, but for $^3\mathrm{He} + \mathrm{Au}$.

can see that for both π^- and π^+, our results fit the E910 data very well, especially at higher momenta. Pion production of the $p + \mathrm{Cu}$ reaction at incident beam momenta of 12.3 and 17.5 GeV/c also fits the E910 data [14] very well. From Fig. 1, we can also see that the cross sections at low angles ($0.9 < \cos\theta < 1$) are evidently larger than those at high angles, especially for energetic pion mesons. As a comparison, we also give the case of $^3\mathrm{He} + \mathrm{Au}$ at the incident beam momentum of 17.5 GeV/c as shown in the bottom panel of Fig. 1. From the bottom panel of Fig. 1, it is seen that differential cross sections of pion production of the ^{3}He-induced reaction are about 5 times those of the proton-induced reaction at an incident beam momentum of 17.5 GeV/c. The cross sections at low angles ($0.9 < \cos\theta < 1$) are also much larger than those at high angles.

To make comparisons systematically between $p + \mathrm{Au}$ and $^3\mathrm{He} + \mathrm{Au}$ at different incident beam energies, we plot Figs. 2–4. From the top panels of Figs. 2–4, we can clearly see that, as the incident beam energy decreases, cross sections of pion production of $p + \mathrm{Au}$ also decrease. This is understandable since pion production mainly comes from decays of resonances and energetic nucleon-nucleon collisions give more resonances. We can also see that, as the beam energy decreases, the energetic pion mesons also decrease rapidly. The bottom panels of Figs. 2–4 are the cases of $^3\mathrm{He} + \mathrm{Au}$ at different incident beam energies. Also we see that, as the beam energy decreases, differential cross sections of pion production decrease rapidly, especially for energetic pion mesons. Compared with $p + \mathrm{Au}$, as the incident beam energy increases, cross sections of pion production at low angles of $^3\mathrm{He} + \mathrm{Au}$ increase more rapidly, especially for energetic pion mesons. In the incident beam energy region from 2.8 to 16.587 GeV/nucleon, cross sections of pion production at low angles ($0.9 < \cos\theta < 1$) and high momentum of $^3\mathrm{He} + \mathrm{Au}$ are 5 to 10 times those of the $p + \mathrm{Au}$ case. Using the AMPT model we also made simulations for $p + \mathrm{Au}$ at incident beam energies from 50 to 100 GeV/nucleon; cross sections of pion production at low angles ($0.9 < \cos\theta < 1$) are about 20 times those of $p + \mathrm{Au}$ at an incident beam energy of 16.587 GeV/nucleon, indicating the saturation of the cross section of pion production at an beam energy of about 50 GeV/nucleon.

We next turn to the study of angle distributions of pion multiplicity of $p + \mathrm{Au}$ and $^3\mathrm{He} + \mathrm{Au}$ at different incident beam energies. From Fig. 5, we can see that for both $p + \mathrm{Au}$ or $^3\mathrm{He} + \mathrm{Au}$, pion emission at low angles increases rapidly, especially at higher incident beam energies. From these plots, we can also see that the low-angle pion emission is more pronounced for $^3\mathrm{He} + \mathrm{Au}$ than for $p + \mathrm{Au}$, especially at

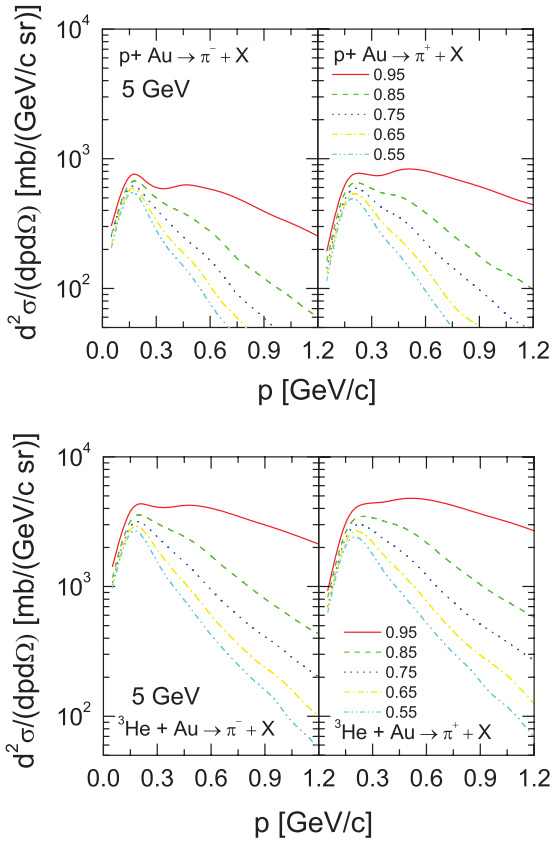

FIG. 3. (Color online) Top: Production cross sections of π^- (left panel) and π^+ (right panel) from p + Au at an incident beam energy of 5 GeV/nucleon shown in bins of $\cos\theta$. Numbers in the legend refer to the center of each bin. Bottom: Same as the p + Au case, but for ^{3}He + Au.

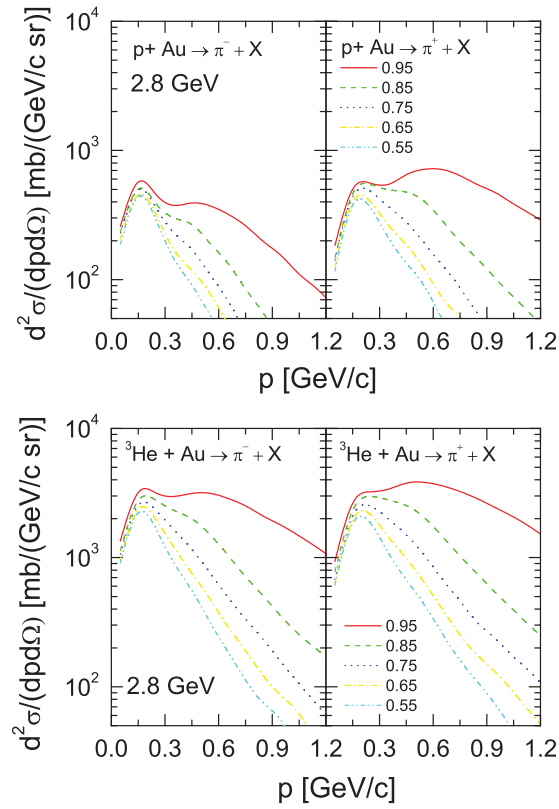

FIG. 4. (Color online) Top: Production cross sections of π^- (left panel) and π^+ (right panel) from p + Au at an incident beam energy of 2.8 GeV/nucleon shown in bins of $\cos\theta$. Numbers in the legend refer to the center of each bin. Bottom: Same as the p + Au case, but for ^{3}He + Au.

higher incident beam energies. Pion numbers from ^{3}He + Au at low angles ($0.9 < \cos\theta < 1$) are about 5 times those of p + Au. This indicates that ^{3}He + Au at a high incident beam energy is more suitable for neutrino experiments compared with p + Au. Figure 6 shows angle distributions of pion relative emitting numbers at different incident beam energies. It is seen that at the high incident beam momentum of 17.5 GeV/c, the relative emitting number at low angles ($0.9 < \cos\theta < 1$) can reach about 50% for ^{3}He + Au. While at the incident beam energy of 2.8 GeV/nucleon, the relative emitting number at low angles ($0.9 < \cos\theta < 1$) reaches only about 25%. At the studied beam energy region, we can clearly see that the ^{3}He-induced reaction on the Au target causes larger proportional low-angle pion emission, especially at higher incident beam energies, about 5% to 10% larger than that of the proton-induced reaction on the Au target.

Figure 7 shows cross sections of charged pion production of p + Au and ^{3}He + Au reactions at different incident beam energies. We can see that, at the incident beam energies studied here, cross sections of pion production of ^{3}He- and proton-induced reactions on the Au target increase about 3 times. The cross sections of ^{3}He-induced reaction on the Au target at the incident beam energy of 2.8 GeV/nucleon are larger than those of the p + Au reaction at the beam energy of 16.587 GeV/nucleon. Figure 8 shows the ratio of cross sections of charged pion production of p + Au and ^{3}He + Au reactions at different incident beam energies. We can clearly see that cross sections of charged pion production from the ^{3}He-induced reaction are about 5

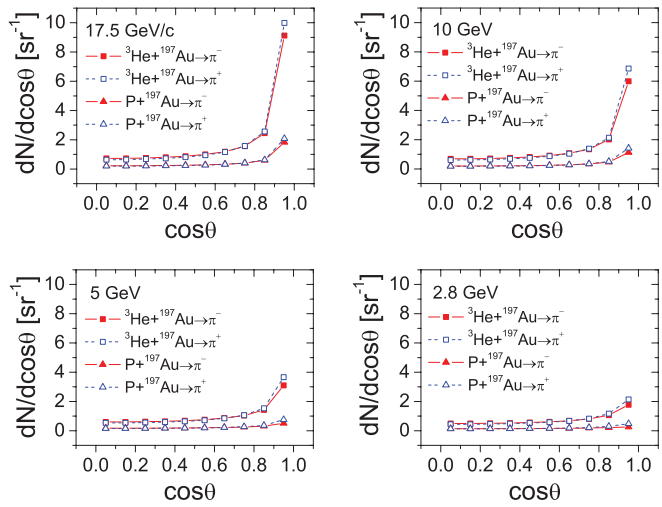

FIG. 5. (Color online) Angle distributions of pion multiplicity of p + Au and ^{3}He + Au at different incident beam energies, in bins of $\cos\theta$.

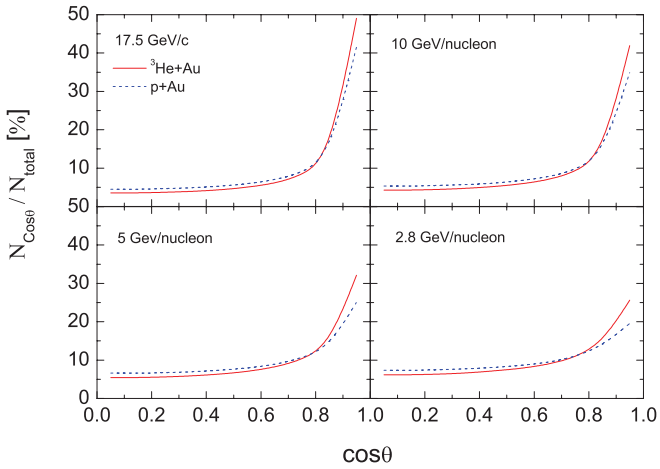

FIG. 6. (Color online) Angle distributions of charged pion relative multiplicity ($N_{\cos\theta}/N_{\text{total}}$) for $p + \text{Au}$ and $^3\text{He} + \text{Au}$ reactions at different incident beam energies, in bins of $\cos\theta$.

times (larger than $A_{^3\text{He}}/A_{\text{H}} = 3$) those of the proton-induced reaction.

Since the work focuses on the proton versus ^{3}He results, one wonders what scaling behavior with projectile nucleon number would one expect from a "standard" cascade model (without mean-field modifications)? Figure 9 shows the ratio of mean pion production per nucleon of projectile with mass number A and 1 (proton) at the incident beam energy of 2.8 GeV/nucleon (by the ART cascade model). We can see that pion production per projectile nucleon is roughly the same with different projectile mass number A, i.e., the produced total pion number is roughly proportional to projectile mass number A. This indicates each nucleon in the projectile excites pion production almost dependently. But for the projectile for which the mass number is smaller than the target mass number, the scaling behavior where total pion number is roughly proportional to projectile mass number A is not strictly correct. In fact, the ratio of $\frac{\pi_A}{\pi_1}/A$ is always larger than 1, as shown in Fig. 9. This is because each nucleon in the projectile does not excite pion production independently. One nucleon in the projectile may give energy to the nucleon in the target,

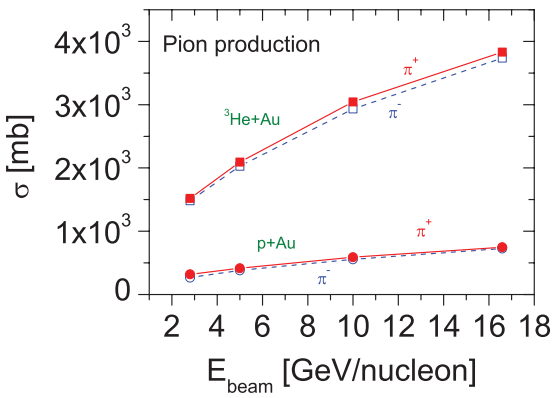

FIG. 7. (Color online) Cross sections of charged pion production of $p + \text{Au}$ and $^3\text{He} + \text{Au}$ reactions at different incident beam energies.

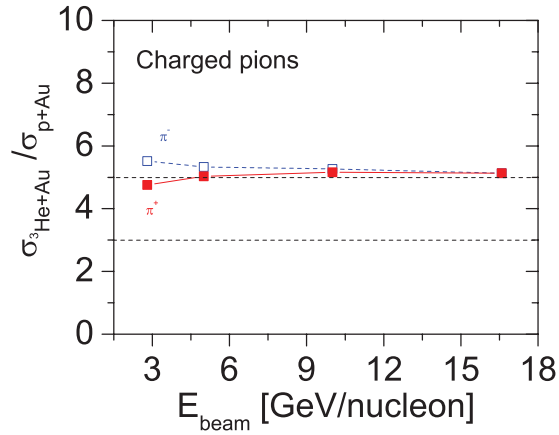

FIG. 8. (Color online) Ratio of cross sections of charged pion production of $p + \text{Au}$ and $^3\text{He} + \text{Au}$ reactions at different incident beam energies.

but does not produce pions. The other nucleon in the projectile may also collide with the nucleon that has obtained energy from the other nucleon of the projectile. Thus the probability of pion production accordingly increases for the other induced nucleon in the projectile. This correlation of different incident nucleons of the projectile does not increase linearly with projectile's mass number due to the marginal collision of the induced nucleon. Thus we see about 5 times pion production of the ^{3}He-induced reaction compared with the proton-induced reaction. For the random impact parameter case, smaller $\frac{\pi_A}{\pi_1}/A$ is due to the marginal collisions of the induced nucleon in the projectile.

To demonstrate neutrino production by proton- or ^{3}He-induced reactions, we plot in Fig. 10 the angle distributions of neutrinos via π^+ decay in proton- and ^{3}He-induced reactions on a Au target. Assuming $\pi^+ \to \mu^+ + \nu_\mu$ and pion decays into μ and ν_μ isotropically in its frame of reference, we can thus obtain neutrino distribution by assuming it rest mass 1 eV. Figure 10 shows angle distributions of neutrino production from positively charged pion dacay in $p + \text{Au}$

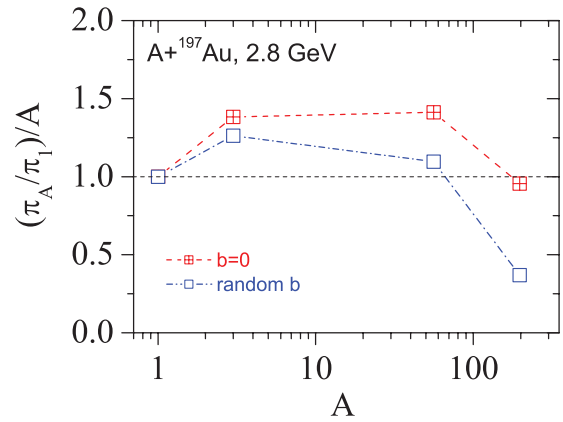

FIG. 9. (Color online) Ratio of mean pion production per nucleon of projectile with mass number A and 1 at the incident beam energy of 2.8 GeV/nucleon. The target is ^{197}Au and the impact parameters are set to be 0 and random, respectively.

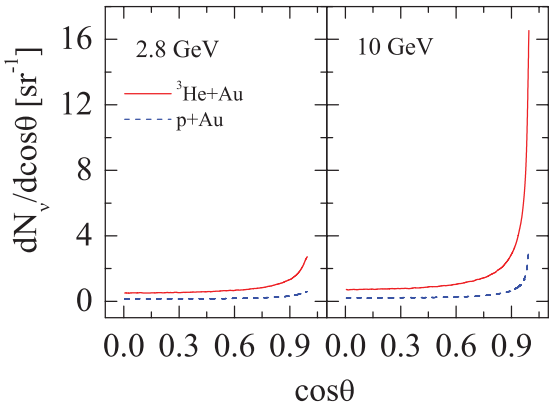

FIG. 10. (Color online) Angle distributions of neutrino production from positively charged pion decay in $p + \mathrm{Au}$ and $^3\mathrm{He} + \mathrm{Au}$ reactions at incident beam energies of 2.8 and 10 GeV/nucleon, in bins of $\cos\theta$.

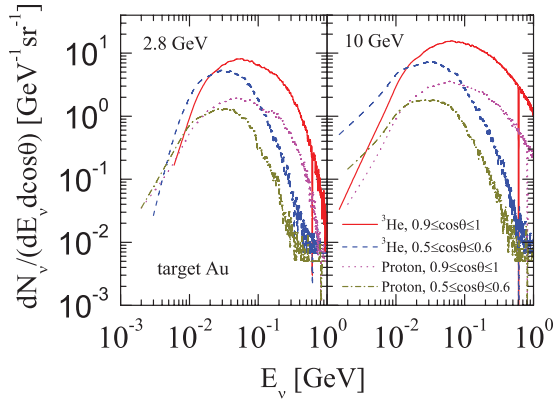

FIG. 11. (Color online) Energy distributions of neutrino production at angles $0.9 < \cos\theta < 1$ and $0.5 < \cos\theta < 0.6$ from positively charged pion decay in $p + \mathrm{Au}$ and $^3\mathrm{He} + \mathrm{Au}$ reactions at incident beam energies of 2.8 and 10 GeV/nucleon.

and ^{3}He + Au reactions at incident beam energies of 2.8 and 10 GeV/nucleon. We can clearly see that neutrinos from the ^{3}He-induced reaction are more inclined to low-angle emission than neutrinos from the proton-induced reaction; this situation is clearer for high incident beam energy. Because the energy distributions of the emitting neutrinos are important for neutrino-nucleus experiments [29–32], we also plot the energy distributions of the produced neutrinos at low and high angles as shown in Fig. 11. We can see that the produced neutrinos possess different energies from about 1 to 1000 MeV and more. The most probable energy is about 30 to 70 MeV for several GeV incident beam energies. Moreover, we can see that neutrinos from low angles possess more energy than those from high angles. Note here that neutrino production can also come from other channels [33], especially for energetic collisions. For physical experiments relevant to neutrinos, detailed studies of the numbers, the energy spectra, and the species of emitted neutrinos are very necessary and therefore the simulations related to neutrino production also become important [33].

IV. CONCLUSIONS

In conclusion, proton- and ^{3}He-induced reactions on ^{197}Au targets at beam energies of 2.8, 5, 10, and 16.587 GeV/nucleon are studied in the framework of the relativistic BUU transport model. It is found that compared with proton-induced reactions, ^{3}He-induced reactions give larger cross sections of pion production, about 5 times those of the proton-induced reactions. Also, ^{3}He-induced reactions are more inclined to low-angle pion emission. Simulations demonstrate that neutrino emission via positively charged pion decay is also inclined to low-angle emission.

ACKNOWLEDGMENTS

The author G. C. Yong acknowledges B. A. Li for providing the ART model code and Z. W. Lin for providing the new version of the AMPT model. The work is supported by the National Natural Science Foundation of China (Grants No. 10635080, No. 10875151, No. Y201260GJ0, No. 10740420550, and No. 10925526), the Knowledge Innovation Project (Grant No. KJCX2-EW-N01) of the Chinese Academy of Sciences, the one Hundred Person Project (Grant No. Y101020BR0), the Major State Basic Research Developing Program of China under Grant No. 2007CB815004, and the CAS/SAFEA International Partnership Program for Creative Research Teams (Grant No. CXTD-J2005-1).

[1] L. Wolfenstein, Phys. Rev. D **17**, 2369 (1978).
[2] L. Wolfenstein, Phys. Rev. D **20**, 2634 (1979).
[3] R. N. Mohapatra and G. Senjanović, Phys. Rev. Lett. **44**, 912 (1980).
[4] Y. Ashie *et al.* (Super-Kamiokande Collaboration), Phys. Rev. Lett. **93**, 101801 (2004).
[5] M. Ambrosio *et al.* (MACRO Collaboration), Phys. Lett. B **566**, 35 (2003).
[6] M. Sanchez *et al.* (Soudan2 Collaboration), Phys. Rev. D **68**, 113004 (2003).
[7] T. Araki *et al.* (KamLAND Collaboration), Phys. Rev. Lett. **94**, 081801 (2005).
[8] M. B. Smy *et al.* (Super-Kamiokande Collaboration), Phys. Rev. D **69**, 011104 (2004).
[9] S. N. Ahmed *et al.* (SNO Collaboration), Phys. Rev. Lett. **92**, 181301 (2004).
[10] E. Aliu *et al.* (K2K Collaboration), Phys. Rev. Lett. **94**, 081802 (2005).
[11] S. Abe *et al.* (KamLAND Collaboration), Phys. Rev. Lett. **100**, 221803 (2008).
[12] A. Strumia and F. Vissani, arXiv:hep-ph/0606054.
[13] J. Collot, H. G. Kirk, and N. V. Mokhov, Nucl. Instrum. Methods Phys. Res., Sect. A **451**, 327 (2000).
[14] I. Chemakin *et al.*, Phys. Rev. C **65**, 024904 (2002).

[15] I. Chemakin *et al*., Phys. Rev. C **77**, 015209 (2008).
[16] M. Apollonio *et al*. (HARP Collaboration), Phys. Rev. C **80**, 065204 (2009) and Refs. [12–21] therein.
[17] S. Agostinelli (GEANT4 Collaboration), Nucl. Instrum. Meth. A **506**, 250 (2003).
[18] N. V. Mokhov and S. I. Striganov, MARS Overview, FERMILAB-CONF-07-008-AD, 2007.
[19] K. Gallmeister and U. Mosel, Nucl. Phys. A **826**, 151 (2009) arXiv:0901.1770.
[20] D. H. Wright *et al*., AIP Conf. Proc. **896**, 11 (2007).
[21] A. Heikkinen *et al*., eConf **C0303241**, MOMT008 (2003).
[22] H. W. Bertini and P. Guthrie, Nucl. Phys. A **169**, 670 (1971).
[23] G. Folger and H. P. Wellisch, eConf **C0303241**, MOMT007 (2003).
[24] S. G. Mashnik *et al*., LANL Report LA-UR-05-7321, 2005.
[25] K. Long, Nucl. Phys. B, Proc. Suppl. **154**, 111 (2006).
[26] G. F. Bertsch and S. Das Gupta, Phys. Rep. **160**, 189 (1988).
[27] B. A. Li and C. M. Ko, Phys. Rev. C **52**, 2037 (1995).
[28] Z.-W. Lin, C. M. Ko, B.-A. Li, B. Zhang, and S. Pal, Phys. Rev. C **72**, 064901 (2005).
[29] K. Kubodera and S. Nozawa, Int. J. Mod. Phys. E **3**, 101 (1995).
[30] E. Kolbe, K. Langanke, G. Martínez-Pinedo, and P. Vogel, J. Phys. G **29**, 2569 (2003).
[31] T. Leitner and U. Mosel, Phys. Rev. C **82**, 035503 (2010); T. Leitner, L. Alvarez-Ruso, and U. Mosel, *ibid*. **73**, 065502 (2006).
[32] A. Y. Illarionov, B. A. Kniehl, and A. V. Kotikov, Phys. Rev. Lett. **106**, 231802 (2011).
[33] A. A. Aguilar-Arevalo *et al*., Phys. Rev. D **79**, 072002 (2009).